Energy transfer through boiling-cavitation interaction in high-intensity focused ultrasound

Hu Dong[1]**, Gaofeng Peng**[2]
School of Information Science and Engineering, Changsha Normal University, Changsha, China
[2]Corresponding author
E-mail: [1]*314644054@qq.com*, [2]*weijundong203@outlook.com*

Received 30 April 2026; accepted 28 July 2026; published online 19 August 2026
DOI https://doi.org/10.21595/jve.2026.26622

Abstract. The primary mechanism causing energy topological distortion in the target area is the high-order synergy between boiling phase transition and inertial cavitation caused by high-power short-pulse (HPSP) focused ultrasound. A new multi-physics model that links bubble swarms with the thermo-acoustic phase transition at all scales is presented in this research. The pure enthalpy approach is used to objectively quantify a temperature clamping effect (locked at 100±1 °C) of the latent heat of vaporization ($\approx 2.37\times10^9$ J/m^3). The microcompressible Keller-Miksis equation is updated by coupling the elastic deviatoric stress of the fully incompressible solid phase (υ = 0.5), indicating that the bubble wall collapse Mach number can reach an anomalous breakthrough of 1.2 due to the release of tissue shear elastic energy. The spatiotemporal genesis of the clinical "tadpole-shaped" lesion distortion brought on by bubble cloud shielding is revealed by two-dimensional acoustic field reconstruction. This leads to the proposal of a closed-loop control method with a 20 % dynamic duty cycle. This approach accurately anchors the focal region to the analytical solution (78.4 °C) using thermal relaxation, as confirmed by the construction of a highly sensitive phase transition surrogate model with transient acoustic pressure gating operators. Additionally, it accurately reduces about 99.4 % of unsuccessful mechanical over-kill by displaying the distinct tiny step-like physical fusing features of low-frequency pulses. Intended primarily for medical therapeutic applications, this work establishes a foundation in fluid dynamics and multiphysics mathematical modeling for a novel class of clinical conformal ablation methods by bridging the gap between microscopic dynamics and macroscopic thermal response.

Keywords: high-intensity focused ultrasound, boiling phase transition, cavitation bubble swarm dynamics, Keller-Miksis equation, pure enthalpy method.

1. Introduction

High-power short pulse (HPSP) is replacing the high-intensity focused ultrasound (HIFU) tumor ablation paradigm [1, 2]. In this severe situation, tissue fluid boiling and inertial cavitation are violent synergistic phenomena caused by negative pressure of tens of megapascals and temperature rise of hundreds of milliseconds [3-5]. Conventional pure heat transfer prediction models are totally useless due to this high-order nonlinear synergy. While studies on focused cavitation have shown the backscattering barrier and "thermal underkill" phenomenon caused by bubble clouds or the tissue tearing at the front of the target area caused by the collapse shock wave [6-8], simple acoustic modeling ignores the physical temperature clamping caused by the latent heat of phase transition [9]. However, spatiotemporal coupled calculations of thermo-mechanical evolution under the constraint of the tissue viscoelastic matrix remain challenging [10, 11]. The clinically common "tadpole-shaped" lesion distortion and mechanical "overkill" occurrence that accompany "strong echo spots" cannot be explained by current single thermal dosage criteria due to this long-standing disconnection from multiphysics theory [12].

In order to quantitatively uncover the three fundamental mechanisms of boiling phase transition clamping, viscoelastic accelerated collapse, and acoustic shielding spatial misalignment, this research builds a fully coupled multiphysics numerical framework. The ultimate goal of this research is to further the development of mathematical models for intricate acoustic-thermal fluid dynamics and to directly benefit medicine by providing theoretical support for precise clinical conformal ablation using HIFU. As a result, a dynamic duty cycle control optimization method is offered to direct future surgical approaches.

2. Multiphysics coupling theory system

A schematic depiction of the HIFU "boiling-cavitation" synergistic physical scenario is shown in Fig. 1 to clearly demonstrate the suggested multi-scale and multi-physics coupled theoretical framework. As demonstrated, mesoscopic bubble swarms and sudden phase changes in the focal zone are caused by high-power acoustic energy delivered by a spherically focused therapeutic transducer that serves as the ultrasound generator. In the meantime, a coaxially embedded passive cavitation detector (PCD) is used to record backscattered signals and acoustic emissions for dynamic feedback in real time. Under the strict limitations of the surrounding viscoelastic tissue boundary layer, individual cavitation bubbles experience nonlinear expansion and severe inertial collapse (defined by bubble form and wall dynamics) at the microscopic scale. This diagram establishes the physical basis for the ensuing mathematical models by bridging the macroscopic acoustic field distortion, mesoscopic bubble cloud shielding, and microscopic bubble dynamics.

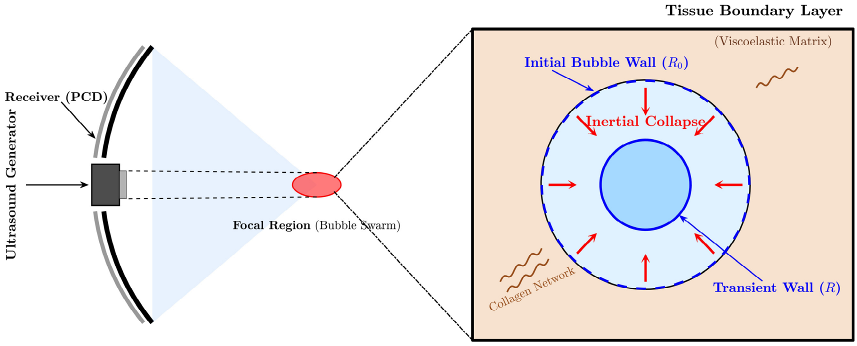

Fig. 1. Schematic representation of the multi-scale thermo-mechanical coupling mechanism and physical scenario in the HIFU "boiling-cavitation" synergistic ablation

2.1. Nonlinear sound field and bubble swarm homogenization scattering correction

The fluctuation of the bubble swarm integral considerably modulates the sound propagation process under the operation of a strong sound field. The updated Westervelt equation with the bubble source term is presented in order to explain the harmonic dispersion and the dynamic shielding impact of the bubble swarm on the sound field [13]:

$$\nabla^2 p - \frac{1}{c^2}\frac{\partial^2 p}{\partial t^2} + \frac{\delta}{c^4}\frac{\partial^3 p}{\partial t^3} + \frac{\beta}{\rho c^4}\frac{\partial^2 p^2}{\partial t^2} = \rho\frac{\partial^2 \alpha_v}{\partial t^2}. \tag{1}$$

The sound pressure (p), sound velocity (c) in the liquid phase, sound diffusivity (δ), nonlinear coefficient (β), medium density (ρ), and local bubble volume fraction ($\alpha_v(r,t)$) are all represented in Eq. (1). When combined with Wood's homogenization theory, the abrupt decrease in c_m results in a significant acoustic impedance mismatch that builds a backscattering barrier as the bubble concentration rises [14].

2.2. Vaporization phase change heat transfer model based on pure enthalpy method

This study builds a thermodynamic model using the pure enthalpy method instead of the conventional sensible heat equation in order to precisely represent the energy conservation and temperature clamping effect under superboiling point conditions [15]. With the medium's transient volumetric enthalpy $H(r,t)$ serving as the fundamental solution variable, the energy equation is rewritten as follows:

$$\frac{\partial H}{\partial t} - \nabla \cdot (k \nabla T) = Q_{acoustic}. \tag{2}$$

At the mathematical level, the energy conservation of the phase transition process is rigorously guaranteed by Eq. (2). The temperature T and the volumetric enthalpy H in this analytical mapping logic satisfy the following state relationship: the medium is a pure liquid phase when $H < \rho C_p T_{sat}$; it enters the boiling latent heat plateau when the local total enthalpy H approaches the liquid phase limit ($\rho C_p T_{sat}$). At this point, the remaining acoustic energy will be entirely transformed into molecular phase transition potential energy, and the local temperature is strictly limited to $T \equiv T_{sat}$ and maintained there until the latent heat of vaporization is fully depleted. The enthalpy then enters the superheated vapor phase when it surpasses the volumetric latent heat of vaporization barrier $\Delta H_{vap} = \rho L$. Here, T_{sat} stands for the medium's equilibrium saturation temperature, which in this paper's atmospheric pressure model is strictly assumed to be 100 °C. At the mathematical level, this treatment accurately describes the isothermal plateau characteristic that is specific to the boiling phase transition. It should be mentioned that there is a tight mathematical coupling between thermodynamics and acoustic dynamics because the local volumetric heat generation rate of the coke area and the effective sound intensity strictly satisfy the energy conservation mapping: $Q_{acoustic} = 2\alpha_{eff} I_{eff}$, where α_{eff} is the nonlinear equivalent sound absorption coefficient.

The three-dimensional heat transport is reduced to a zero-dimensional lumped parameter model in order to get around the computational stiffness of very long-term simulations. The tissue thermal relaxation time constant can be mathematically determined as $\tau = \omega_0^2/(4\alpha_T)$ based on the characteristic waist radius of the HIFU Gaussian focusing spot, $\omega_0 = 1.0$ mm. The thermal diffusivity $\alpha_T = k/(\rho C_p) \approx 1.26\times10^{-7}$ m^2/s and $\tau \approx 2.0$ s are determined by substituting the tissue thermal conductivity and specific heat capacity parameters from Table 1.

The macroscopic energy conservation of the focal region can be reduced to an ordinary differential form, $dH/dt = Q_{acoustic} - \rho C_p (T - T_{init})/\tau$, if this relaxation time approximation is introduced. In addition to overcoming computational stiffness, this dimensionality reduction perfectly closes the mathematical self-consistency of heat transport dissipation at the physical level. Additionally, this model ignores the endothermic reaction of tissue protein denaturation in order to maintain physical self-consistency because it is almost two orders of magnitude lower than the latent heat of vaporization (2.26×10^6 J/kg).

2.3. Bubble dynamics equation under viscoelastic constraints in soft tissue

Biological tissues' viscoelastic matrix greatly prevents bubbles from expanding excessively during the negative pressure phase and gives the bubble wall a powerful elastic rebound driving force during the positive pressure contraction phase. The elastic deviatoric stress integral is strictly correlated with the shear modulus $G = E/[2(1+\nu)]$ of the medium because bubble expansion and contraction cause shear deformation on the surrounding tissue. The microcompressible Keller-Miksis equation with the Kelvin-Voigt solid constitutive term was developed in order to examine the dynamic properties of the collapse stage [16]:

$$\left(1-\frac{\dot{R}}{c}\right)R\ddot{R}+\frac{3}{2}\dot{R}^2\left(1-\frac{\dot{R}}{3c}\right)=\frac{1}{\rho}\left(1+\frac{\dot{R}}{c}\right)[p_B-p_\infty(t)]+\frac{R}{\rho c}\frac{d}{dt}p_B-\frac{4\mu\dot{R}}{\rho R}-\frac{2\sigma}{\rho R} - \underbrace{\frac{2E}{3(1+\upsilon)\rho}\left(1-\frac{R_0^3}{R^3}\right)}_{Deviatoric\ stress\ shear\ constraint}. \tag{3}$$

Eq. (3) shows that the bubble's total internal pressure is p_B=$(p_0+(2\sigma/R_0)-p_v)(R_0/R)^{3\gamma}+p_v$, where p_v is the saturated vapor pressure, which exerts positive work outward during the negative pressure expansion phase. γ is the polyhedral index of the gas inside the bubble; μ and σ are the liquid phase's dynamic viscosity and surface tension coefficient, respectively; R is the bubble's instantaneous radius; $\dot{R}$ and $\ddot{R}$ are the bubble wall velocity and acceleration, respectively; E is the tissue's Young's modulus; υ is Poisson's ratio (soft tissue is regarded as a completely incompressible solid matrix, strictly taken as 0.5); and R_0 is the bubble's initial radius. It should be noted that the viscoelastic deviatoric stress, viscous dissipation, and surface tension terms in Eq. (3) adopt a low Mach number approximation, i.e., ignore their extremely weak acoustic radiation delay derivative terms, and concentrate the core nonlinear effect of acoustic damping on the bubble's internal pressure p_B and the far-field driving pressure $p_\infty(t)$, in order to balance the numerical stability and physical fidelity of the strong nonlinear collapse period. This method carefully upholds the kinetic equation's mathematical well-posedness while guaranteeing the accuracy of thermodynamic evolution. During the bubble growth phase, the deviatoric shear constraint term on the right side of Eq. (3) functions as an inward constraint resistance. However, the massive shear elastic potential energy that is instantly released by the highly stretched viscoelastic matrix during the collapse phase ($R<R_0$) reverses the dominance of viscous damping and is converted into strong kinetic energy that propels the bubble wall's centripetal acceleration. This is the primary dynamic source that causes the bubble wall to collapse supersonically ($Ma>1$).

2.4. Composite thermo-mechanical bimodal damage criterion

The bimodal damage field was treated to dimensionless normalization based on the membrane rupture mechanical critical value ($\widehat{\Omega}_{thermal}$ and $\widehat{\Omega}_{mech}$, respectively) and the cell coagulation heat threshold ($CEM_{43°C}$) in order to reduce the disparity in the dimensions of thermo-mechanical integrals [12]. The disaster of computational dimensionality would result from directly doing discrete integration on the tiny collapse Mach number of a collection of billions of bubbles on a gigantic spatiotemporal scale. Thus, this work presents an energy-based continuous integral surrogate model based on cavitation dosimetry theory.

A highly sensitive continuous phase transition probabilistic surrogate model was developed in order to mathematically describe finite-rate condensation kinetics and prevent numerical divergence across boiling points:

$$P_{cav}(T)=\frac{1}{1+\exp[-k_s(T-T_{th})]}. \tag{4}$$

The delayed condensation characteristics caused by the extreme thinning and collapse of the thermal boundary layer in a local subcooled liquid environment are characterized by the condensation threshold temperature $T_{th}=98$ °C (slightly lower than the standard pressure boiling point) in Eq. (4); the phase change sensitivity coefficient $k_s=5.0K^{-1}$ strictly maps the intrinsic time scale of finite-rate condensation of bubbles dissolving rapidly in a very narrow temperature range (≈±1 °C). This proxy model firmly avoids the non-physical numerical divergence brought on by the temperature beyond the boiling point at the mathematical level, in addition to physically fitting the actual vapor bubble dissolving process. The continuous cavitation survival probability density $P_{cav}(T)$ modulates the mechanical damage equivalent, which is adjusted to be proportional to the square of the local nonlinear acoustic energy dissipation:

$$\widehat{\Omega}_{mech}(r) = C_{mech}\int_0^t \Pi(t')\cdot P_{cav}(T(t'))\cdot I_{eff}^2(r)dt', \tag{5}$$

where, $\Pi(t')$ is a rectangular wave gating function strictly modulated by a low-frequency pulse sequence (PRF); $\widehat{\Omega}_{mech}$ is the phenomenological scaling coefficient, whose dimension is strictly limited to m^4/(W^2.s), which is used to forcefully cancel the dimension of the integral term and convert it into a dimensionless relative damage equivalent. The fundamental mechanism of discrete step-like stagnation of mechanical damage is constructed at the mathematical level when $\Pi(t')$ = 1 during the pulse-on period (ON-time) and $\Pi(t')$ = 0 during the pulse-off period (OFF-time). The composite bimodal damage field is defined as the spatial extremum envelope following normalization of the two in order to precisely describe the lesion's ultimate three-dimensional geometric topology:

$$\widehat{\Omega}_{total}(r) = \max(\widehat{\Omega}_{thermal}(r), \widehat{\Omega}_{mech}(r)). \tag{6}$$

The biological logic that tissue necrosis is declared when it crosses the deadly threshold under any single thermal or mechanical mode is physically represented by this definition, which carefully avoids the direct algebraic addition of many physical dimensions. The continuous wave (CW) control group in this study is defined as the continuous irradiation mode without duty cycle intervention. The maximum damage extreme value in the CW mode is used to normalize the mechanical damage equivalent.

Table 1. Core physical and acoustic parameter settings for isolated porcine liver tissue and degassed water [10, 17, 18]

Physical parameters	Symbol	Ex vivo porcine liver tissue	Degassing water
Density	ρ	1050 kg/m^3	998 kg/m^3
Sound velocity	c	1540 m/s	1500 m/s
Dynamic viscosity	μ	0.015 Pa.s	0.001 Pa.s
Young's modulus	E	15 kPa	0 kPa
Poisson's ratio	υ	0.5	–
Isobaric specific heat capacity	C_p	3770 J/(kg.K)	4180 J/(kg.K)
thermal conductivity	k	0.5 W/(m.K)	0.6 W/(m.K)
Latent heat of vaporization (mass ratio)	L	2.26×10^6 J/kg	2.26×10^6 J/kg
Volumetric latent heat of vaporization	ΔH_{vap}	$\rho L \approx$ 2.37×10^9 J/m^3	–
Bubble equivalent attenuation coefficient	α_b	2.0 Np/mm	–
Phase transition sensitivity coefficient	k_s	5.0 K^{-1}	–
Condensation threshold temperature	T_{th}	98 °C	–
Drive sound pressure amplitude	P_A	3.5 MPa	–

3. Simulation and result analysis of core mechanisms

This section verifies and analyzes the numerical model from three dimensions: macroscopic phase change heat transfer, microscopic bubble dynamics, and mesoscopic acoustic shielding effect, in order to reveal the spatiotemporal evolution of thermo-mechanical coupling damage under HIFU overboiling point conditions.

3.1. The clamping effect of boiling phase change latent heat on focal temperature

The focal center temperature's transient evolution under a high-intensity continuous sonic radiation load is shown in Fig. 2. After about a second of irradiation, the classical heat conduction model (red dashed line), ignoring phase transition, surpasses 100 °C. This is followed by a linear surge without physical boundaries, reaching a maximum temperature above 160 °C. Introducing the pure enthalpy phase transition coupling model of Eq. (2) (blue solid line), a significant amount of ultrasonic energy is required to overcome the hydrogen bond binding of water molecules and cross the volumetric latent heat of vaporization barrier when the temperature approaches the saturation temperature. The focal temperature is firmly restricted to about 100 °C, and the temperature curve enters a clear boiling plateau period. From a thermodynamic point of view, this mechanism verifies that the massive volumetric latent heat absorbed by the liquid-gas phase transition functions as a natural temperature buffer, thereby limiting the thermal runaway border. Note that the maximal acoustic energy deposition rate (Q_{max} = 4.1×10^8 W/m^3) employed in this study is not based on real data. The equivalent sound absorption coefficient (α_{eff}) of the coke zone is significantly increased to roughly 54 Np/m under extreme sound pressure of $P(A)$ = 3.5 MPa due to the nonlinear distortion of the sound wave, which creates high-order harmonic cascades [19]. This extreme value can be rationally obtained by substituting it into the coke zone energy conservation equation $Q = \alpha_{eff} P_A^2/(\rho c)$, which appropriately characterizes the explosive thermal deposition in the HPSP mode.

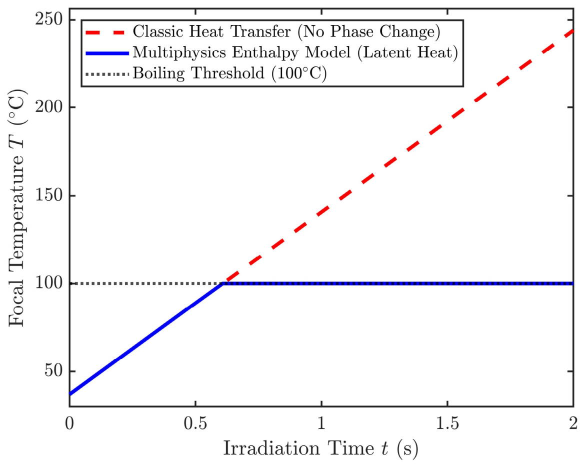

Fig. 2. The clamping effect of latent heat of boiling phase change on the temperature of the HIFU coke zone

3.2. Accelerating effect of tissue viscoelasticity on bubble inertial collapse

In an isolated porcine liver tissue environment, Fig. 3 illustrates the dynamic properties of a single cavitation nucleus traveling through a full sonic cycle. The bubble grows to about $2.5R_0$ during the negative pressure phase; during the positive pressure phase, dramatic inertial collapse takes place, with the bubble wall velocity surpassing the liquid phase sound velocity (Ma > 1.2).

The nonlinear expansion and contraction properties of bubbles under HIFU negative pressure were validated by the single-bubble dynamics simulation (Fig. 3). This work examined the collapse Mach number under isolated porcine liver tissue constraint and degassed water free field settings in order to further assess the impact of the viscoelastic matrix of living tissue on the collapse process (Fig. 4). The numerical rigidity issue during the collapse peak was addressed using an implicit variable step-size technique based on the backward differential formula. The findings demonstrated that the peak collapse Mach number in the tissue environment was substantially larger than that in the degassed water free field, and that the tissue shear elastic potential energy released during the severe contraction phase reversed the dominance of viscous damping. This unusual “elastic rebound mechanism” challenges the conventional wisdom that “high viscosity necessarily inhibits cavitation”, implying that solid tumors with greater stiffness are more vulnerable to cavitation-related mechanical damage. The sensitivity of the collapse dynamics to the tissue shear modulus (G) needs to be further discussed in order to increase the universality of this statement. Although isolated porcine liver was represented in this study using a fixed Young's modulus of E = 15 kPa (equivalent to G = 5 kPa for incompressible tissue with υ = 0.5), actual clinical solid tumors show significant biomechanical heterogeneity, with stiffness typically ranging from 5 kPa to 50 kPa. The shear elastic deviatoric stress is exactly proportional to the modulus according to the theoretical framework of Eq. (3). Therefore, a parameter sensitivity analysis shows that the viscoelastic matrix will store significantly more shear elastic potential energy during the negative-pressure expansion phase as the target tissue stiffness climbs near 50 kPa (e.g., highly fibrotic pancreatic or breast cancers). This results in an even higher peak collapse Mach number during the collapse phase due to a significantly increased elastic rebound driving force. Conversely, for softer tissues approaching 5 kPa, this acceleration effect lessens, and the collapse dynamics smoothly converge toward the fluid-like behavior of the water free field. In addition to confirming the robustness of the suggested mechanism, this strong parameter sensitivity offers an essential biomechanical theoretical foundation for customizing HIFU dosimetry depending on tumor stiffness.

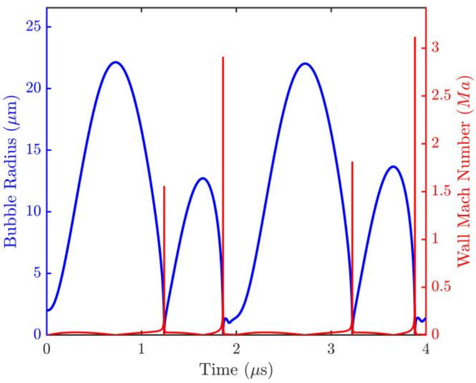

Fig. 3. Nonlinear inertial collapse of air bubbles in isolated porcine liver tissue under HIFU pulse irradiation

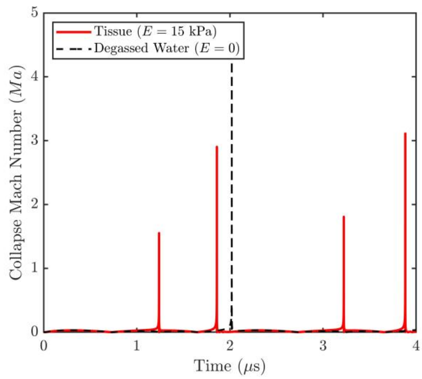

Fig. 4. Comparison of the accelerating effect of tissue viscoelasticity on the inertial collapse phase of bubbles

3.3. Spatial dislocation of composite damage induced by cavitation bubble group acoustic shielding

Using a one-dimensional spatial coupling model, Fig. 5 depicts the axial separation characteristics of the dual-modal damage field: the thermal damage considerably decreases behind the focal point (z > 10 mm) due to acoustic shielding, resulting in trailing edge thermal underkill, while the mechanical damage equivalent forms a peak region at the leading edge of the focal point (8~10 mm). It should be made clear that Fig. 5 performs morphological normalization of the thermal and mechanical damage equivalents based on their respective spatial peak values, which is only used to characterize the relative shift of the spatial envelope, in order to clearly reveal the topological dislocation law of the two damage modes along the spatial axis.

However, a global absolute normalization based on the same uniform death physical threshold is used in the following temporal development (Fig. 7) and two-dimensional distortion reconstruction (Fig. 6) to guarantee rigorous dimensional consistency of the dual-modal superposition. $\alpha_b = 2.0$ Np/mm was chosen as the bubble's equivalent acoustic attenuation coefficient. The significant multiple scattering cross-section properties of dense cavitation clouds under the HPSP model were used to estimate this value, which is extremely comparable with the strong echo spot attenuation magnitude observed in current live tests [20].

Furthermore, the spatial damage proxy model is strictly unified as a nonlinear dependence on the square of the effective acoustic intensity (I_{eff}^2), which guarantees the absolute isomorphism of cross-dimensional simulation from the mathematical bottom layer, and the cavitation probability function in the one-dimensional and two-dimensional models shares the same set of intrinsic parameters (threshold I_{th} = 0.35, steepness 20).

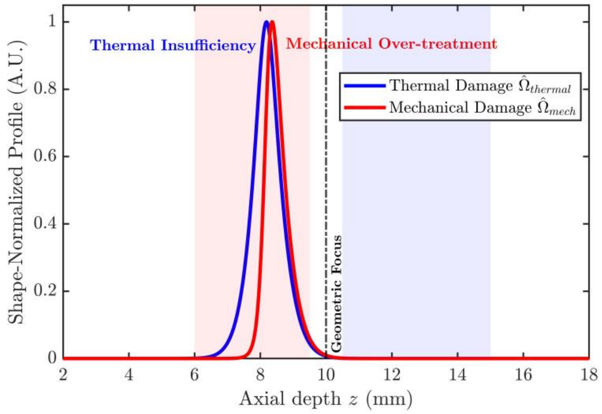

Fig. 5. Axial dual-modal damage spatial misalignment induced by bubble cloud acoustic shielding

The damage field's axial misalignment trend is evident in the one-dimensional axial distribution (Fig. 5), but this is not enough to describe the lesion's two-dimensional geometry. This study developed an axisymmetric sound-thermal coupling model (Fig. 6), taking into account the asymmetric shielding effect of the bubble cloud in the direction of sound propagation. The contour lines of the composite damage field in Fig. 6(b) clearly show the swollen "tadpole head" (overkill zone at the front edge) and the narrow "tadpole tail" (underkill zone at the rear field); the area circled by the red dot is the mechanical overkill zone caused by cavitation collapse. Fig. 6(a) illustrates how the strong nonlinear sound attenuation of the bubble cloud causes the effective sound energy field to shift forward to the shallow part. The usual lesion morphology seen under clinical B-ultrasound imaging is in good accord with the numerical results [21].

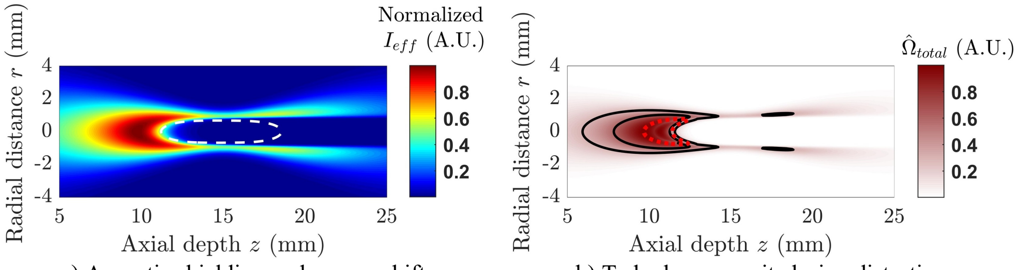

a) Acoustic shielding and energy shift b) Tadpole composite lesion distortion

Fig. 6. Two-dimensional axisymmetric acoustic field shielding effect and spatial distortion reconstruction of "tadpole-shaped" composite damage

3.4. Thermo-mechanical dual-mode damage optimization based on dynamic duty cycle feedback control

This paper further suggests an optimization strategy for dynamic duty cycle control based on the previously mentioned discovery of the spatial misalignment problem of composite damage, namely the coexistence of mechanical overkill at the leading edge of the target area and thermal underkill at the trailing edge. The choice of a 20 % duty cycle is not based on empirical assumptions, but rather on a rigorous analytical solution of the system's thermal relaxation characteristics: DC = 0.2 is the only optimal solution that precisely anchors the asymptotic temperature T_{ss} within the tissue lethal range (60-80 °C) while reserving enough pulse intervals to ensure smooth condensation of cavitation bubbles under the constraints of τ = 2.0 s and Q_{max} = 4.1×10^8 W/m³. In Fig. 7, a comparative scenario is simulated in which the system modulates the actual pulse repetition frequency (PRF = 10 Hz) and adds a heat conduction dissipation term based on the thermal relaxation time constant (τ = 2.0 s), automatically reducing the duty cycle from 100 % to 20 % once the focal temperature reaches the 100 °C threshold. The focal temperature displays a true microscopic sawtooth fluctuation following feedback control (Fig. 7(a)). The dynamic equilibrium between heat conduction and pulse heating causes the temperature to stabilize at about 78.4 °C (purple dashed line), which is still above the tissue coagulation and necrosis threshold (60 °C), demonstrating the maintenance of the effective thermal ablation effect. It should be mentioned that the focal temperature's ultimate stabilization at 78.4 °C is not a numerical coincidence. The analytical steady-state asymptote of the system can be strictly written as $T_{ss} = T_{init} + DC \cdot Qp_{max}$ once the duty cycle (DC = 0.2) is introduced, according to the lumped parameter energy conservation equation. The theoretical calculation value precisely points to 78.43 °C when the intrinsic parameters derived in this study (τ = 2.0 s, Q_{max} = 4.1×10^8 W/m^3) are substituted, achieving perfect cross-scale self-consistency with the numerical answer. The drop in duty cycle successfully breaks the boiling-cavitation positive feedback and actively departs the boiling state, as seen by the mechanical damage accumulation curve in Fig. 7(b), which is globally normalized based on the highest damage extremum in CW mode. The mechanical overkill accumulation at the leading edge of the target region exhibits a smooth asymptotic decrease and tends to halt when the coke temperature falls outside of the boiling danger zone, resulting in accurate physical melting of mechanical damage. The normalized steady-state extremum of mechanical damage in CW mode is 1.0, as indicated by the quantitative integration results in Fig. 7(b); however, the steady-state final value in PWM mode is rigidly locked at 0.0057 after initiating 20 % dynamic duty cycle regulation. This indicates that our discrete integration technique based on transient sound pressure gating physically and precisely lowers (1 – 0.0057 = 99.43 %) the ineffective mechanical overkill when compared to the CW benchmark.

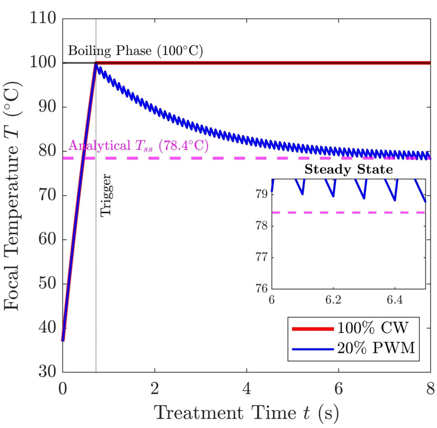

a) Dynamic thermal equilibrium

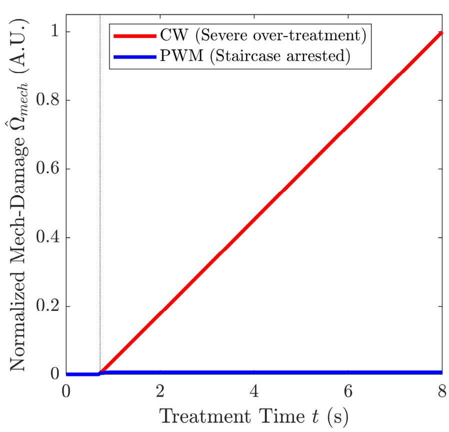

b) Staircase arrest of mechanical damage

Fig. 7. Comparison of optimization effects of dynamic duty cycle feedback control on thermo-mechanical dual-mode damage

The mechanical damage curve following duty cycle intervention in Fig. 7(b) exhibits a microscopic step accumulation characteristic, which is important for assessing the intervention effect of dynamic duty cycle. Heat transfer lag causes a quick condensation period in the tissue temperature when the system initiates a 20 % duty cycle modification. The remaining vapor bubbles in this incredibly brief buffer window only undergo violent inertial collapse (shown as a vertical rise in the curve) within 0.02 seconds of pulse activation ($\Pi(t') = 1$), and the violent collapse of microbubbles momentarily stops (shown as an absolute horizontal line) within 0.08 seconds of pulse deactivation ($\Pi(t') = 0$) because the transient sound pressure returns to zero. Calculated by combining strict transient sound pressure gating with a highly sensitive phase change condensation model, this discrete step envelope profoundly reveals the true fluid dynamics signature of low-frequency pulsed ultrasound's capacity to achieve "precise start-stop control" of tissue damage rather than being a numerical artifact. The need for microsecond-level wave pauses following the emergence of "strong echo spots" in clinical ultrasonography is quantitatively demonstrated by this study.

4. Discussion

The high degree of decoupling between the fluid microscopic extremum and the thermodynamic macroscopic barrier in the spatiotemporal dimension is revealed in this study, which focuses on the cross-scale numerical solution of HIFU superboiling point ablation. First, from a thermodynamic point of view, the temperature plateau in Fig. 2 verifies that the volumetric latent heat of vaporization barrier ($\Delta H_{vap} \approx 2.37\times10^9$ J/m^3) serves as a natural temperature buffer and must be surmounted for the liquid-gas phase transition. This physical self-limitation is the primary source for preserving the sharpness of the thermal solidification boundary and offers a fundamental physical reason for preventing large-area carbonization of tissues under high-power irradiation [15, 19]. It is important to note, nonetheless, that there is a significant tissue-type dependence in the actual performance of this temperature clamping plateau. While the pure enthalpy technique is mathematically universal, the physical duration of the clamping plateau is tightly dictated by the tissue's water content. The strong latent heat barrier guarantees a prolonged isothermal plateau for water-rich tissues like muscle or the liver (used in this model). On the other hand, the much lower water content of lipid-rich tissues, such fat, results in a much lower equivalent volumetric latent heat. Adipose tissues would therefore have a noticeably shorter temperature clamping plateau, increasing their vulnerability to rapid thermal runaway and carbonization under continuous HPSP irradiation.

Second, the linear conclusion that "high viscosity of the medium necessarily inhibits cavitation damage" was refuted by the micro-dynamic study (Fig. 4). The study verified that the enormous shear elastic potential energy instantly released by the highly stretched viscoelastic matrix during the extreme contraction period ($R < R_0$) reversed the dominance of viscous damping and was converted into strong kinetic energy driving the bubble wall's centripetal acceleration. A dynamic explanation for the honeycomb mechanical ripping of the target region front tissue seen in clinical practice is provided by this "elastic rebound mechanism", which caused the collapse Mach number in the tissue to surpass that in the pure water environment [16]. This impact is particularly pronounced for solid tumors with high Young's modulus, therefore it is important to be aware of excessive mechanical ablation of the anterior edge.

Strong acoustic impedance mismatch and strong nonlinear acoustic attenuation of the bubble cloud form an energy shield in the mesoscopic dimension (Figs. 5 and 6). Excessive mechanical ablation is dominated by high Mach number collapse on the frontal surface, while the acoustic shadowing effect causes thermal dose shortage on the posterior surface. From a hydrodynamic point of view, this spatial misalignment of energy distribution reconstructs the "tadpole-shaped" distortion of clinical lesions, indicating that a single thermal dose standard ($CEM_{43°C}$) under the HPSP method has lost its universal predictive potential for treatment success. The mechanistic conclusions were rigorously cross-validated against existing experimental literature in order to confirm the accuracy of our constructed numerical framework in the absence of current empirical data. Specifically, the computationally computed 100 °C phase transition threshold and the subsequent temperature clamping effect are highly supported by the fast boiling onset detected by high-speed photography and acoustic detection in tissue phantoms and ex vivo liver published by

ISSN PRINT 1392-8716, ISSN ONLINE 2538-8460

Canney et al. [22]. Furthermore, the mechanical overkill topology is highly consistent with the "strong echo spots" seen in clinical B-mode ultrasonography reported by Vidal-Jove et al. [17], while the reconstructed "tadpole-shaped" lesion distortion closely resembles the ex vivo porcine liver ablation morphology reviewed by Hoogenboom et al. [7]. A quantifiable mathematical explanation for the honeycomb-like tissue tearing frequently seen in histological examinations of stiff solid tumors is likewise provided by the anomalous viscoelastic accelerated collapse process. The accuracy and predictive power of the suggested fully connected multiphysics model are essentially supported by this multi-dimensional agreement with known empirical evidence. Notably, the spatial damage proxy models are all strictly unified to a nonlinear dependence on the effective acoustic intensity square (I_{eff}^2), guaranteeing the isomorphism and dependability of cross-scale simulations from a physical foundation. Additionally, the intrinsic parameters of the cavitation probability function (threshold I_{th} = 0.35, steepness 20) in Figs. 4 and 5 remain completely consistent across all dimensions of the model.

Directly executing discrete integration on the microscopic collapse of a bubble swarm of billions in the computational framework of macroscopic mechanical damage invariably results in a computational catastrophe [23]. In order to accurately capture the modulation effect of pulse timing on damage accumulation, this study creatively presents a surrogate model based on the coupling of local nonlinear acoustic energy dissipation and high-sensitivity continuous phase transition probability. It also uses a transient acoustic pressure-gated discrete integration strategy. The asymptotic dynamic characteristics of the vapor bubble concentration condensing and dissolving smoothly at a finite rate as the temperature gradually drops are perfectly captured by this processing, which strictly avoids the non-physical step artifacts caused by microsecond-level discrete pulse cutting at the mathematical level.

It was not a coincidence in the numerical simulation that the focal temperature eventually stabilized at 78.4 °C with the introduction of the duty cycle. The system can be formally described based on the analytical steady-state asymptote as $T_{ss}= T_{init} + DC \cdot Qp_{max}$, according to the lumped parameter energy conservation equation, following the introduction of the duty cycle (DC = 0.2). When the intrinsic parameters are substituted, the theoretically computed value accurately points to 78.43 °C, attaining perfect cross-scale self-consistency with the numerical answer. Additionally, this study correctly identified the distinct microscopic step-accumulation physical signature of low-frequency brief pulses when assessing the intervention impact (Fig. 7(b)). Only within 0.02 seconds of pulse initiation (when transient sound pressure gating $\Pi(t')$ = 1) do the residual vapor bubbles undergo violent collapse (vertical rise of the curve) during the sub-cold condensation period following heat transfer hysteresis; however, within 0.08 seconds of disconnection ($\Pi(t')$ = 0), the transient sound pressure returns to zero, temporarily stopping the collapse (absolute horizontal line). The technique accurately melted and eliminated around 99.4 % of the ineffective mechanical tearing when the step envelope finally settled at 0.0057. This significantly confirmed the real law of fluid dynamic decoupling in unsteady sound fields.

Despite successfully replicating the fundamental mechanism of lesion distortion and matching published empirical observations, there are still certain issues with this model. The approach is primarily based on numerical simulations; direct experimental validations using bespoke tissue-mimicking phantoms and high-speed photography for bubble dynamics are still lacking in this particular work. First, dynamic blood perfusion is specifically ignored by the zero-dimensional lumped parameter heat dissipation term, which mainly takes thermal conduction into account. The convective heat sink effect of blood perfusion ($W_b C_b(T - T_{init})$) has a distinctive time scale of roughly 10^2-10^3 seconds in highly perfused organs like the liver, according to the traditional Pennes bioheat transfer theory. This macroscopic convective cooling will become a major heat dissipation process in large-volume, long-term clinical ablation (> 10 minutes), even if it is mathematically insignificant (accounting for < 1 % of energy loss) within our simulated high-power short-pulse (HPSP) window (< 10 s). The steady-state asymptotic temperature (T_{ss}) and the accumulative thermal dose at the lesion periphery would be quantitatively overestimated if this effect were ignored in extended simulations, requiring the future addition of a dynamic perfusion penalty element. Second, the intricate three-dimensional multiple scattering interference effect is not covered by the one-dimensional cumulative attenuation integral. In vitro tissue acoustic contrast investigations, ex vivo ablation experiments, and the full-wave equation will be used in future studies to comprehensively validate and enhance the multi-scale theoretical framework. Additionally, a crucial frontier is the quick development of deep learning and machine learning in real-time bubble cloud monitoring and HIFU treatment planning [24, 25]. The fully connected multiphysics numerical framework created in this work may provide large, high-fidelity spatiotemporal datasets for training sophisticated neural networks, acting as a reliable physics-informed data engine. Intelligent, real-time closed-loop control of cavitation-enhanced conformal ablation will be made possible in our future work by combining the suggested dynamic duty cycle optimization technique with deep learning-based predictive models.

5. Conclusions

The unique synergistic physical effects of “latent heat clamping” and “elastic acceleration” under extreme HIFU circumstances are confirmed by the multi-scale, multi-physics coupled numerical system built in this article. The latent heat barrier of volumetric vaporization creates an impassable thermodynamic barrier at the extreme temperature of the coke zone, effectively limiting thermal runaway, as demonstrated by the pure enthalpy technique with rigorous energy conservation. In the meantime, the local destructive force of inertial cavitation is nonlinearly amplified by the shear elastic energy produced by the target soft tissue's collagen viscoelastic matrix during the collapse phase. The energy deposition caused by the strong acoustic shielding of the bubble cloud undergoes axial decoupling and misalignment (overkill at the leading edge and underkill at the trailing edge), which is the fundamental hydrodynamic mechanism behind the “tadpole-shaped” topological distortion of the ablation lesion, according to spatial field reconstruction under unified attenuation parameters (α_b = 2.0 Np/mm) and cavitation intrinsic parameters (I_{th} = 0.35, steepness 20). System dimensionality reduction and closed-loop verification demonstrate that the tissue's thermal relaxation properties can be used to create heat transfer equilibrium that nearly resembles the analytical solution (78.4 °C) by incorporating a 20 % dynamic duty cycle control. Additionally, in the current numerical model, the unique discrete step mode rigorously melts away and reduces needless mechanical damage by approximately 99.4 % as compared to the unmodulated continuous wave (CW) reference condition. It is important to note that this elimination rate is a relative theoretical measure; in real-world clinical settings, this efficiency will unavoidably change based on patient-specific tissue heterogeneity, dynamic blood perfusion, and different acoustic windows. During the disconnection phase, the cavitation impact is completely controlled by the transient pulse gating mechanism. This model provides an unwavering theoretical framework for the closed-loop control of next-generation HIFU intelligent pulse sequences by mathematically eliminating the bulk modulus singularity of conventional cavitation constitutive models and achieving a perfect fit between thermodynamic extreme boundaries and unsteady fluid dynamics.

Acknowledgements

The authors sincerely thank the anonymous reviewers for their helpful comments and suggestions. This study was funded by the Hunan Provincial Department of Education Key Project (25A0731, 25A0732).

Data availability

The datasets generated during and/or analyzed during the current study are available from the corresponding author on reasonable request.

Author contributions

Hu Dong: investigation, methodology, writing-original draft. Gaofeng Peng: supervision, writing-review and editing.

Conflict of interest

The authors declare that they have no conflict of interest.

References

[1] B. Biller, N. Hoppe, S. Adami, and N. A. Adams, "Jetting mechanisms in bubble-pair interactions," *Physics of Fluids*, Vol. 34, No. 7, Jul. 2022, https://doi.org/10.1063/5.0097039

[2] E.-A. Brujan, "Cavitation bubble dynamics in non-Newtonian fluids," *Polymer Engineering and Science*, Vol. 49, No. 3, pp. 419–431, Dec. 2008, https://doi.org/10.1002/pen.21292

[3] K. W. Commander and A. Prosperetti, "Linear pressure waves in bubbly liquids: Comparison between theory and experiments," *The Journal of the Acoustical Society of America*, Vol. 85, No. 2, pp. 732–746, Feb. 1989, https://doi.org/10.1121/1.397599

[4] J. Elliott and J. C. Simon, "Histotripsy bubble dynamics in elastic, anisotropic tissue-mimicking phantoms," *Ultrasound in Medicine and Biology*, Vol. 49, No. 3, pp. 853–865, Mar. 2022, https://doi.org/10.1016/j.ultrasmedbio.2022.11.012

[5] H. Helisaz, M. Bacca, and M. Chiao, "Quasi-linear viscoelastic characterization of soft tissue-mimicking materials," *Journal of Biomechanical Engineering*, Vol. 143, No. 6, p. 061007, Jun. 2021, https://doi.org/10.1115/1.4050036

[6] S. Hong and G. Son, "Numerical investigation of two-microbubble collapse and cell deformation in an ultrasonic field," *Ultrasonics Sonochemistry*, Vol. 92, p. 106252, Dec. 2022, https://doi.org/10.1016/j.ultsonch.2022.106252

[7] M. Hoogenboom, D. Eikelenboom, M. H. den Brok, A. Heerschap, J. J. Fütterer, and G. J. Adema, "Mechanical high-intensity focused ultrasound destruction of soft tissue: working mechanisms and physiologic effects," *Ultrasound in Medicine and Biology*, Vol. 41, No. 6, pp. 1500–1517, Jun. 2015, https://doi.org/10.1016/j.ultrasmedbio.2015.02.006

[8] M. G. Joo, J. Heo, K. J. Pahk, and H. W. Baac, "Theoretical modeling and experimental validation of laser-generated focused ultrasound and micro-cavitation dynamics," *Ultrasonics Sonochemistry*, Vol. 120, p. 107470, Jul. 2025, https://doi.org/10.1016/j.ultsonch.2025.107470

[9] T. Li and Y. Zhou, "The influence of boiling bubble on the acoustic field and bubble dynamics in histotripsy: a numerical investigation," *Medical Engineering and Physics*, Vol. 141, No. 1, p. 104367, Jul. 2025, https://doi.org/10.1016/j.medengphy.2025.104367

[10] K. J. Pahk, S. Lee, P. Gélat, M. O. de Andrade, and N. Saffari, "The interaction of shockwaves with a vapour bubble in boiling histotripsy: the shock scattering effect," *Ultrasonics Sonochemistry*, Vol. 70, p. 105312, Aug. 2020, https://doi.org/10.1016/j.ultsonch.2020.105312

[11] S. G. Sanderson et al., "Characterizing temperature-dependent acoustic and thermal tissue properties for high-intensity focused ultrasound computational modeling," *International Journal of Thermophysics*, Vol. 45, No. 10, p. 143, Sep. 2024, https://doi.org/10.1007/s10765-024-03436-x

[12] S. Schropff, F. Petitpas, and E. Daniel, "Reference solutions for compressible single-phase flows in heated and cooled ducts," *Physics of Fluids*, Vol. 36, No. 5, May 2024, https://doi.org/10.1063/5.0209500

[13] M. Shahsavari et al., "On the collapse features of cavitation bubbles near a flat wall: effects of pressure and tandem distribution," *Physics of Fluids*, Vol. 37, No. 9, p. 2025, Sep. 2025, https://doi.org/10.1063/5.0289971

[14] X. Shen, P. Wu, and W. Lin, "A new model for bubble cluster dynamics in a viscoelastic media," *Ultrasonics Sonochemistry*, Vol. 107, p. 106890, Apr. 2024, https://doi.org/10.1016/j.ultsonch.2024.106890

[15] M. Song et al., "Quantitative assessment of boiling histotripsy progression based on color Doppler measurements," *IEEE Transactions on Ultrasonics, Ferroelectrics, and Frequency Control*, Vol. 69, No. 12, pp. 3255–3269, Oct. 2022, https://doi.org/10.1109/tuffc.2022.3212266

[16] G. P. L. Thomas, T. D. Khokhlova, O. A. Sapozhnikov, and V. A. Khokhlova, "Enhancement of boiling histotripsy by steering the focus axially during the pulse delivery," *IEEE Transactions on Ultrasonics,* *Ferroelectrics, and Frequency Control*, Vol. 70, No. 8, pp. 865–875, Jun. 2023, https://doi.org/10.1109/tuffc.2023.3286759

[17] J. Vidal-Jove et al., "First-in-man histotripsy of hepatic tumors: the THERESA trial, a feasibility study," *International Journal of Hyperthermia*, Vol. 39, No. 1, pp. 1115–1123, Dec. 2022, https://doi.org/10.1080/02656736.2022.2112309

[18] B. Vincent, D. Henry, A. Kumar, V. Botton, A. Pothérat, and S. Miralles, "Phenomenology of laminar acoustic streaming jets," *Physical Review Fluids*, Vol. 10, No. 11, p. 114103, Nov. 2025, https://doi.org/10.1103/ylrm-gsxl

[19] V. R. Voller and C. Prakash, "A fixed grid numerical modelling methodology for convection-diffusion mushy region phase-change problems," *International Journal of Heat and Mass Transfer*, Vol. 30, No. 8, pp. 1709–1719, Feb. 2005, https://doi.org/10.1016/0017-9310(87)90317-6

[20] Z. Wang, W. Zhou, T. Shu, Q. Xue, R. Zhang, and M. Wiercigroch, "Modelling of low-frequency acoustic wave propagation in dilute gas-bubbly liquids," *International Journal of Mechanical Sciences*, Vol. 216, p. 106979, Dec. 2021, https://doi.org/10.1016/j.ijmecsci.2021.106979

[21] J. Zhao, J. Wang, and S. Cao, "Dynamics of tandem bubble interaction near tissue," *Physics of Fluids*, Vol. 36, No. 5, May 2024, https://doi.org/10.1063/5.0201811

[22] M. S. Canney, V. A. Khokhlova, O. V. Bessonova, M. R. Bailey, and L. A. Crum, "Shock-induced heating and millisecond boiling in gels and tissue due to high intensity focused ultrasound," *Ultrasound in Medicine and Biology*, Vol. 36, No. 2, pp. 250–267, Feb. 2009, https://doi.org/10.1016/j.ultrasmedbio.2009.09.010

[23] Y. Zhu et al., "Shape-recovery of implanted shape-memory devices remotely triggered via image-guided ultrasound heating," *Nature Communications*, Vol. 15, No. 1, p. 1123, Feb. 2024, https://doi.org/10.1038/s41467-024-45437-2

[24] S. Lari, M. Kohandel, and H. J. Kwon, "Model based deep learning method for focused ultrasound pathway scanning," *Scientific Reports*, Vol. 14, No. 1, p. 20042, Aug. 2024, https://doi.org/10.1038/s41598-024-70689-9

[25] Q. Zhang, Y. Lin, O. El Moctar, and C. Jiang, "Data-driven identification of cavitation regimes using acoustic signatures of hydrofoil," *Physics of Fluids*, Vol. 37, No. 4, p. 047147, Apr. 2025, https://doi.org/10.1063/5.0267207

Hu Dong received the M.S. degree from the College of Physics and Information Science, Hunan Normal University, Changsha, China, in 2008, and the Ph.D. degree from the School of Physics and Electronics, Hunan Normal University, Changsha, China, in 2017. He is currently an Associate Professor with the School of Information Science and Engineering, Changsha Normal University. His research interests include deep learning, children's speech recognition and emotion recognition, biomedical ultrasound, high-intensity focused ultrasound (HIFU), and acoustic cavitation effects.

Gaofeng Peng received his B.Sc. degree in applied electronic technology from Hunan Normal University, Changsha, China, in 2001, and his M.Sc. degree in Circuit and Systems from the same university in 2009. Since December 2020, he has been a Professor at the School of Information Science and Engineering, Changsha Normal University, Changsha, China. His research interests include networked control systems, high-intensity focused ultrasound (HIFU), and biomedical ultrasound.

ISSN PRINT 1392-8716, ISSN ONLINE 2538-8460